Environmental Pollution 247 (2019) 1020–1027

Contents lists available at ScienceDirect

Environmental Pollution

journal homepage: www.elsevier.com/locate/envpol

Characterization of interactions between a metabolic uncoupler O-chlorophenol and extracellular polymeric substances of activated sludge☆

Fang Fang [a, b, *], Run-Ze Xu [a], Su-Na Wang [a], Lu-Lu Zhang [a], Yan-Qiu Huang [a], Jing-Yang Luo [a], Qian Feng [a], Jia-Shun Cao [a]

[a] Key Laboratory of Integrated Regulation and Resource Development on Shallow Lakes, Ministry of Education, College of Environment, Hohai University, Nanjing, 210098, China
[b] Guangzhou Key Laboratory of Environmental Exposure and Health, School of Environment, Jinan University, Guangzhou, 510632, China

ARTICLE INFO

Article history:
Received 25 October 2018
Received in revised form
30 January 2019
Accepted 3 February 2019
Available online 5 February 2019

Keywords:
Activated sludge
Extracellular polymeric substances
Interaction mechanism
Metabolic uncoupler
Spectral methods

ABSTRACT

Metabolic uncouplers are widely used for the in-situ reduction of excess sludge from activated sludge systems. However, the interaction mechanism between the metabolic uncouplers and extracellular polymeric substances (EPS) of activated sludge is unknown yet. In this study, the interactions between a typical metabolic uncoupler, o-chlorophenol (oCP), and the EPS extracted from activated sludge were explored using a suite of spectral methods. The binding constants calculated for the four peaks of three-dimensional excitation-emission matrix fluorescence were in a range of $1.24–1.76 \times 10^3$ L/mol, implying that the tyrosine protein-like substances governed the oCP-EPS interactions. Furthermore, the results of Fourier transform infrared spectroscopy, X-ray photoelectron spectroscopy and ^{1}H nuclear magnetic resonance indicated that the carboxyl, carbonyl, amine, and hydroxyl groups of EPS were the main functional groups involved in the formation of the oCP-EPS complex. The results of this study are useful for understanding the interactions between metabolic uncouplers and the EPS of activated sludge as well as their fates in biological wastewater treatment systems.

1. Introduction

The activated sludge process is widely used in wastewater treatment plants (WWTPs) for treating both municipal and industrial wastewaters (Liu, 2003). However, long-term performance of activated sludge systems can be constrained by production of excess sludge (Gostomski and Vela, 2018). The treatment and disposal of excess sludge may account for 50–60% of the total operational costs of a WWTP (Guo et al., 2013). Thus, development of effective in situ or post-sludge reduction strategies is essential. Among these available strategies, dosing metabolic uncouplers is regarded as promising in situ sludge reduction strategy because of its high efficiency, easy operation, and consistent system configuration (Guo et al., 2013; Fang et al., 2015; Li et al., 2016a,b; Gostomski and Vela, 2018). Previous studies have shown that various metabolic uncouplers, such as 2,4-dinitrophenol (dNP), para-nitrophenol (pNP), 2,4-dichlorophenol (dCP), o-chlorophenol (oCP), 3,3′,4',5-tetrachlorosalicylanilide (TCS), and tetrakis (hydroxymethyl) phosphonium sulfate (THPS), were effective in reducing sludge production at both lab and pilot scales (Guo et al., 2014; Fang et al., 2015; Li et al., 2016a,b; Ferrer-Polonio et al., 2017).

Extracellular polymeric substances (EPS), which fill the space between microbial cells, are sticky solid materials secreted by microorganisms for maintaining and protecting the structure and strength of microbial aggregates (Sheng et al., 2010). EPS are mainly composed of polysaccharides, proteins, nucleic acids and heteropolymers and account for 50–90% of total organic carbon in the activated sludge (Wei et al., 2011). The presence of various functional groups in EPS provides the binding sites for the adsorption of pollutants, such as antibiotics, heavy metals, and metabolic uncouplers, thereby affecting the transport, persistence and bioavailability of pollutants in activated sludge systems (Sheng

☆ This paper has been recommended for acceptance by Charles Wong.

* Corresponding author. Key Laboratory of Integrated Regulation and Resource Development on Shallow Lakes, Ministry of Education, College of Environment, Hohai University, Nanjing, 210098, China.
E-mail address: ffang65@hhu.edu.cn (F. Fang).

https://doi.org/10.1016/j.envpol.2019.02.005
0269-7491/

et al., 2010; Xu et al., 2013; Zhang et al., 2018). In previous studies, the impacts of metabolic uncouplers on the reduction of excess sludge are usually the research focus (Guo et al., 2014; Fang et al., 2015; Ferrer-Polonio et al., 2017). Studies on the investigation into the interaction between metabolic uncouplers and EPS of activated sludge are very limited.

Recently, the interaction mechanisms between EPS and various pollutants in wastewater were investigated. It was found that electrostatic interactions and complexing bonds were the main mechanisms for the binding reactions between heavy metals and EPS (Sheng et al., 2013). Differently, hydrophobic interaction was the main driving force for the binding process between EPS and micro-pollutants like sulfamethizole (Xu et al., 2013; Wang et al., 2018a). However, the interaction mechanism between metabolic uncouplers and the EPS of activated sludge remains poorly understood.

Therefore, the aim of this study was to explore the interaction between metabolic uncouplers and extracted EPS. A typical metabolic uncoupler, o-chlorophenol (oCP), was selected as the target uncoupler. The solubilizing EPS were extracted from activated sludge. The reaction mechanism between oCP and extracted EPS was investigated using UV–vis and three-dimensional excitation-emission matrix (3D-EEM) fluorescence spectroscopic technologies. The variation of the functional groups in the interaction was examined by using Fourier transform infrared spectroscopy (FTIR), X-ray photoelectron spectroscopy (XPS), and nuclear magnetic resonance (NMR). In this way, useful information on the interaction mechanism between metabolic uncouplers and EPS could be provided.

2. Materials and methods

2.1. Seed sludge and wastewater

The seed sludge was obtained from the Northern Municipal Wastewater Treatment Plant in Wuxi City, China. Then, it was cultivated in a 12-L sequencing batch reactor (SBR), which was operated in a continuously aerated mode at $30\pm1^{\circ}C$ by using a water bath. The reactor was operated sequentially within a 6-h cycle, including feeding (5 min), aeration (320 min), settling (15 min), withdrawal (5 min) and idle phase (15 min). The hydraulic and sludge retention times were maintained at 12 h and 15 d, respectively. The pH of the feed solution was adjusted at 7.0 ± 0.2, and the pH in the reactor was not controlled during the cultivation period. The dissolved oxygen (DO) concentration was kept above 3 mg/L through supplying air, and a stirrer was used to mix the bulk liquid completely.

A synthetic wastewater was used throughout the experiments, which was composed of sodium acetate (400–1000 mg COD/L), NH_4Cl (92–153 mg/L), KH_2PO_4 (17.5–43.8 mg/L), $MgSO_4$ (15 mg/L), $CaCl_2$ (20 mg/L), and $FeSO_4$ (15 mg/L). In addition, other minerals were added, including H_3BO_3 (50 $\mu g/L$), $ZnCl_2$ (50 $\mu g/L$), $CuCl_2$ (30 $\mu g/L$), $MnSO_4 \cdot H_2O$ (50 $\mu g/L$), $(NH_4)_6Mo_7O_{24} \cdot 4H_2O$ (50 $\mu g/L$), $AlCl_3$ (50 $\mu g/L$), $CoCl_2 \cdot 6H_2O$ (50 $\mu g/L$), and $NiCl_2$ (50 $\mu g/L$). The activated sludge was acclimated for two months and the mixed liquid suspended solid (MLSS) level was maintained at approximately 3000 mg/L prior to the experiments.

2.2. EPS extraction

EPS were extracted using the cation exchange resin (CER, Amberlite 732, sodium form) method as described by Frølund et al. (1996). A total of 3000 mL of the sample was taken from the SBR at the end of the aeration stage and then were centrifuged at 5000 rpm, 4 °C for 15 min. The sludge pellets were washed twice with a 100 mmol/L NaCl solution. After each wash, the centrifugation was performed to remove the supernatant at 5000 rpm, 4 °C for 15 min. Later, the sludge pellets were resuspended to their original volume (3000 mL) with a phosphate buffer. The mixture was transferred to a conical flask and the CER (60 g/g VSS) was added. The suspension was stirred for 6 h at 4 °C and centrifuged at 10000 rpm, 4 °C for 30 min. Thereafter, the supernatant was filtered using a 0.45 μm Millipore filter and saved as the EPS for the subsequent experiments.

2.3. Experimental setup and sampling

Our previous study has proven that 5–20 mg/L of oCP could effectively reduce sludge production (Fang et al., 2015). To further investigate the interaction between oCP and EPS, the ranges of 5–20 mg/L of oCP were selected in this study. First, the different oCP concentrations of 5, 10, 15, and 20 mg/L were prepared by diluting oCP solution with deionized water for UV–vis analysis. Then, five beakers were prepared, each of which was filled with 250 mL of the extracted EPS samples. Later, o-chlorophenol of different volumes was added to make a final o-chlorophenol concentration of 0, 5, 10, 15, and 20 mg/L in the five beakers. The mixture was mixed by a magnetic stirrer for 4 h. Then, samples were collected to measure the polysaccharides, proteins and humic compounds, and for UV–vis, EEM, FTIR, XPS, and NMR analyses. The concentrations of polysaccharides, proteins and humic acids of the pristine EPS were measured as 35.98 ± 3.66, 46.00 ± 1.67 and 10.38 ± 2.08 mg COD/L, respectively.

2.4. Analytical methods

The polysaccharide contents were determined by the anthrone method using glucose as a standard (Sheng et al., 2005). The contents of proteins and humic acids were determined using the corrected Lowry method (Raunkjær et al., 1994). Egg albumin was used as the standard for the measurements of proteins, and humic acids was used for the determination of humic compounds.

A UV–vis spectrometer Alpha-1506 (PuYuan Co., China) was used to detect the UV–vis absorption spectra (200–700 nm) of all samples with a 0.1 nm-step. The fluorescence EEMs of the samples were recorded using a fluorescence spectrometer F-7000 (Hitachi Co., Japan) with excitation (Ex) wavelengths ranging from 200 to 600 nm at a 10 nm-interval and emission (Em) wavelengths ranging from 200 to 600 nm at a 2 nm scanning step. Excitation and emission slits were both maintained at 5 nm and the scanning speed was 12000 nm/min.

The EPS samples were freeze-dried by a vacuum freeze dryer (Labconco Inc., USA). Then, the freeze-dried samples were analysed by FTIR Nexus 870 (Thermo Nicolet Inc., USA). The FTIR spectra were obtained over a frequency range from 4000 to 400 cm^{-1} and the resolution was set as 2 cm^{-1}. The amide I region of EPS at 1700-1600 cm^{-1} was further analysed to extract protein secondary structures. The overlapped peaks with the minimum residual were resolved by using the Peakfit software (Version 4.12, Seasolve Software Inc., USA).

XPS PHI 5000 (VersaProbe Co., USA) with an Al Kα X-ray source ($h\nu = 1486.6$ eV) was used to determine the elemental composition and functional groups of the EPS samples. In each measurement, the X-ray source and the beam spot were set as 25 W and 100 μm, respectively. All binding energies were calibrated using the neutral C1s peak at 284.6 eV. The XPS analysis consisted of a broad survey scan (187.85 eV pass energy) for analyzing the main element composition and a high-resolution scan (58.7 eV pass energy) for determining the component speciation.

^{1}H NMR spectra were recorded on a NMR spectrometer DRX500

(Bruker Co., USA) equipped with a 5 mm inverse probe with a z-gradient coil at 500 MHz at room temperature. The freeze-dried EPS samples were dissolved in 0.5 mL D_2O (99.9%) for data acquisition in 5 mm NMR tubes.

3. Results and discussion

3.1. UV–Vis conformational changes of EPS caused by oCP

The UV–Vis adsorption spectroscopy was applied to examine the conformational changes of EPS due to different oCP concentrations. The characteristic peaks of oCP in deionized water were located at 215 nm and 273 nm (Fig. 1A). The 215 nm peak was assigned to E_2 band of phenol, while the peak at 273 nm was attributed to the presence of oCP aromatic rings (Shi et al., 2012; Mal et al., 2017). In Fig. 1B, the UV–vis spectra of the pristine EPS also had two peaks. The peak at 231 nm was assigned to $n \rightarrow \pi^*$ transition of the amide bond (Havel, 1996), and the band around 270 nm was possibly ascribed to phenyl group of tryptophan residues (Trp) and tyrosine in EPS (Mandal et al., 2009). To extract the change of UV–vis spectral response to oCP dosing, the UV–vis spectral data of deionized water with corresponding concentrations of oCP were subtracting from the spectral data of EPS with different concentrations of oCP (Habibul & Chen, 2018). The differential log-transformed forms of UV–vis spectral were shown in Fig. 1C. On gradual addition of oCP to EPS solution, the absorbance of the band situated at 215 nm decreased and the absorbance of the band around 252–270 nm fluctuated slightly, indicating that the interaction between oCP and tryptophan and tyrosine proteins in EPS occurred.

3.2. Fluorescence quenching mechanism for the EPS-oCP interaction

3D-EEM was used to characterize the chemical composition with fluorescence characteristics contained in the EPS. The fluorescence peak positions and fluorescence intensity in the EEM spectra are presented in Fig. 2 and Table S1, respectively. As illustrated in Fig. 2, four main peaks (I-IV) were observed. Peak I, situated at 230/300–305 nm, was attributed to the tyrosine amino acid, while Peak II, located at 225–230/345-355 nm, was assigned to the tryptophan amino acid. Peak III, located at 270–275/355-360 nm, belonged to the tryptophan protein-like substances, while Peak IV, located at 280/310 nm, was attributed to the tyrosine protein-like substances (Chen et al., 2003). The four peaks intensity in the 3D-EEM spectra of EPS decreased with the increasing oCP concentration, indicating the occurrence of fluorescence quenching. Previous studies have demonstrated that the strong hydrophobic protein-like substances in EPS could provide many active sites for the adsorption of organic micro-pollutants (Sheng et al., 2010; Song et al., 2014). The presence of tryptophan- and tyrosine-like substances facilitated the adsorption of ciprofloxacin onto the EPS extracted from activated sludge (Zhang et al., 2018). Thus, the fluorescence quenching mechanism was explored to elucidate the changes in the conformational structure of the fluorophore in EPS.

The widely used fluorescence quenching processes include dynamic and static quenching processes. The diffusive collision between the excited fluorophore and quencher results in the dynamic quenching process, while the complexation between fluorophore and quencher leads to the static quenching process (Song et al., 2010). The Stern-Volmer equation (Eq. (1)) was used to describe the dynamic fluorescence quenching process:

$$\frac{F_0}{F} = 1 + K_{SV}[Q] = 1 + K_q \tau_0 [Q] \quad (1)$$

where F_0 is the fluorescence intensity of the pristine EPS; and F is the fluorescence intensities of EPS in the presence of oCP with different concentrations (5–20 mg/L). K_{SV} denotes the Stern-Volmer quenching constant, K_q is the quenching rate constant of the biological macromolecule, τ_0 of 10^{-8} s represents the average lifetime of the molecule in the absence of quencher, and [Q] is the concentration of the oCP (Hu et al., 2005).

The estimated K_{SV} values from the Stern-Volmer equation for Peaks I, II, III and IV were 1.85×10^3, 2.05×10^3, 1.55×10^3 and 1.26×10^3 L/mol, respectively, with the corresponding K_q values

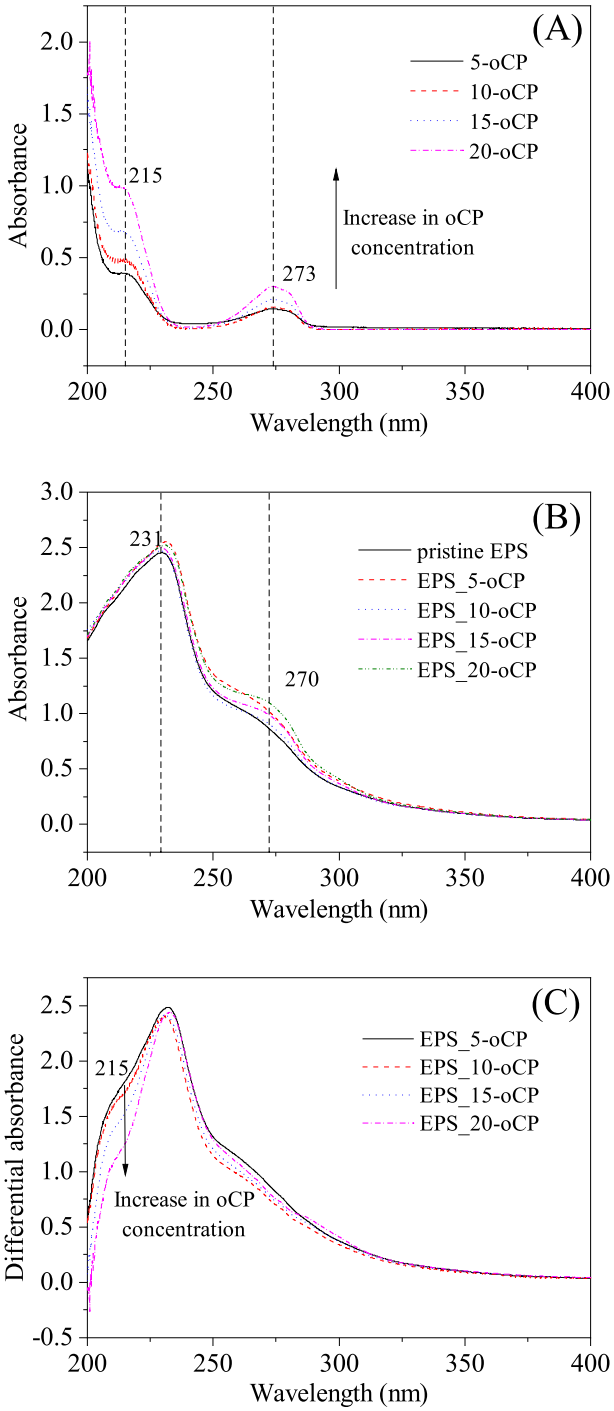

Fig. 1. UV–Vis spectra of (A) oCP at different concentrations, (B) EPS reacting with oCP at different concentrations, and (C) Differential log-transformed absorption spectra of EPS with oCP at different concentrations.

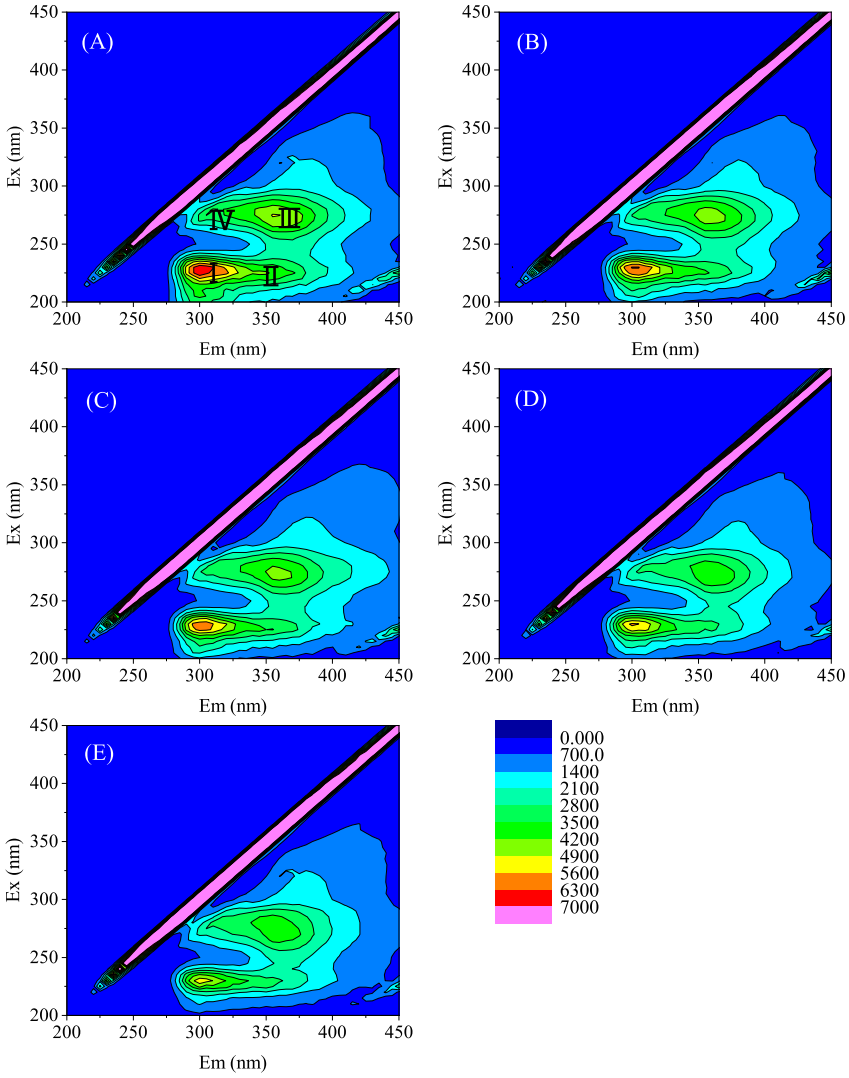

Fig. 2. 3D-EEM spectra of EPS reacting with oCP at different concentrations, (A) the pristine EPS, (B) EPS_5-oCP, (C) EPS_10-oCP, (D) EPS_15-oCP, and (E) EPS_20-oCP.

calculated at 1.85×10^{11}, 2.05×10^{11}, 1.55×10^{11} and 1.26×10^{11} L/mol/s. The quenching constants for EPS and oCP were all higher than the maximum diffusion collision quenching rate constant (2.0×10^{10}) (Xu et al., 2013). This result implies that the fluorescence quenching of EPS by oCP might be caused by the formation of a complex, i.e., EPS-oCP, rather than collision quenching.

The static fluorescence quenching process could be described by the modified Stern-Volmer equation:

$$\frac{F_0}{F_0 - F} = 1 + \frac{1}{K_A[Q]} \tag{2}$$

where K_A is the effective quenching constant for the accessible fluorophores.

The estimated K_A values from the modified Stern-Volmer equation for Peaks I, II, III and IV were 2.09×10^3, 6.46×10^3, 2.24×10^3, and 1.44×10^3 L/mol, respectively, which were close to the values (2.4×10^3 L/mol) reported for the binding of 2,6-dichlorophenol to EPS (Li et al., 2016a,b). These results indicate that the four fluorescent substances had a strong binding ability to oCP.

Fluorescence intensity data were used to estimate the binding constant (K_b) and the number of binding sites (n) for EPS binding to oCP using the Hill equation (Wang et al., 2018b):

$$log\frac{F_0 - F}{F} = logK_b + nlog[Q] \tag{3}$$

where K_b is the binding constant, and n is the number of binding sites.

The binding constants K_b for Peaks I, II, III and IV were 1.76×10^3, 1.28×10^3, 1.24×10^3, and 1.25×10^3 L/mol, respectively, and the binding sites n for Peaks I, II, III and IV were 0.99, 0.60, 0.87, and 0.96, respectively. The binding site number n values for Peaks I and IV were close to 1, indicating that one class of binding sites of the tyrosine protein-like substances present in EPS was involved in trapping oCP, and the binding of oCP to EPS was mainly governed by the tyrosine protein-like substances in EPS.

3.3. Functional groups involved in the formation of the EPS-oCP complex

The FTIR spectra of the pristine EPS and EPS_20-oCP are illustrated in Fig. 3. The infrared spectrum of EPS exhibited a broad band at 3378 cm^{-1}, which was attributed to the stretching vibrations of both O–H (of the polysaccharides) and N–H (of the proteins). The

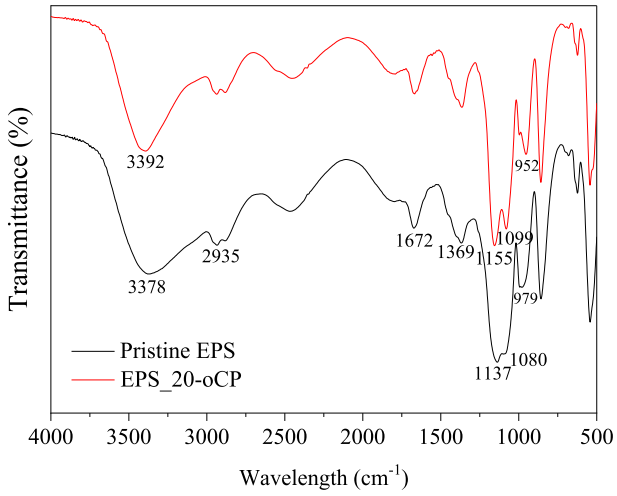

Fig. 3. FTIR spectra of the pristine EPS and EPS_20-oCP.

weak peak at 2935 cm^{-1} corresponded to the C—H stretching vibration (Song et al., 2014). The amide I band at 1672 cm^{-1} was assigned to C=O stretching vibrations in proteins, and the band at 1369 cm^{-1} was caused by the symmetric stretching vibration of C=O in $-COO^-$ groups (Yuan et al., 2011). The bands at 1099 cm^{-1} and 1137 cm^{-1} originated from the C—O—C ring and C—O stretching vibrations in polysaccharides (Wang et al., 2012; Song et al., 2014). The band at 979 cm^{-1} was ascribed to sulfate groups (C—O—S bond) in EPS (Xiao et al., 2018).

After EPS reacted with the oCP, the shape and intensity of several characteristic peaks in the FTIR spectrum changed. The broad band at 3378 cm^{-1} turned to a narrow band at 3392 cm^{-1}, indicating that the hydroxyl groups in EPS and oCP were involved in the interactions. The bands at 1080 cm^{-1} and 1137 cm^{-1} were shifted to 1099 cm^{-1} and 1155 cm^{-1}, respectively, caused by the interactions between carboxyl groups (C—O) in EPS and oCP. In addition, the intensity of peaks at 2935 cm^{-1}, 1672 cm^{-1} and 1369 cm^{-1} decreased, implying that carbonyl groups (C=O) contributed to the coordination of oCP with EPS. These observations suggest that the hydroxyl, carboxyl, and carbonyl groups in EPS were the main functional groups involved in EPS-oCP complex formation.

The protein secondary structures were analysed to further understand the role of proteins in the interactions between EPS and oCP. The secondary structure of amide I was assigned to the specified region (Beech et al., 1999). The curve fitting of the original spectra is presented in Fig. 4, and the detailed information of band assignments are listed in Table 1. The amide I in the pristine EPS and EPS_20-oCP included the tyrosine side chain (1607–1603 cm^{-1}), aggregated strands (1626–1616 cm^{-1}), β-sheet (1640–1629 cm^{-1}), α-helix (1650–1649 cm^{-1}), 3-turn helix (1671–1659 cm^{-1}), and antiparallel β-sheet (1691–1678 cm^{-1}). The protein secondary structure of random coils (1645–1640 cm^{-1}) was absent in the pristine EPS and EPS_20-oCP. Among all the protein secondary structures, the 3-turn helix was the main protein secondary structure (34.55–35.58%) of the EPS samples. After reacting with oCP, the percentage of β-sheets in the EPS increased from 10.94% to 22.40%, while the percentage of antiparallel β-sheets decreased from 29.47% to 18.89%. With an increase in β-sheet secondary structure in the extracellular proteins, the inner hydrophobic groups could be more readily exposed, leading to a higher hydrophobicity of EPS (Jia et al., 2017). According to previous studies (Yin et al., 2015; Xing et al., 2018), certain protein secondary structures, such as aggregated strands, β-sheets, and α- and 3-turn helices,

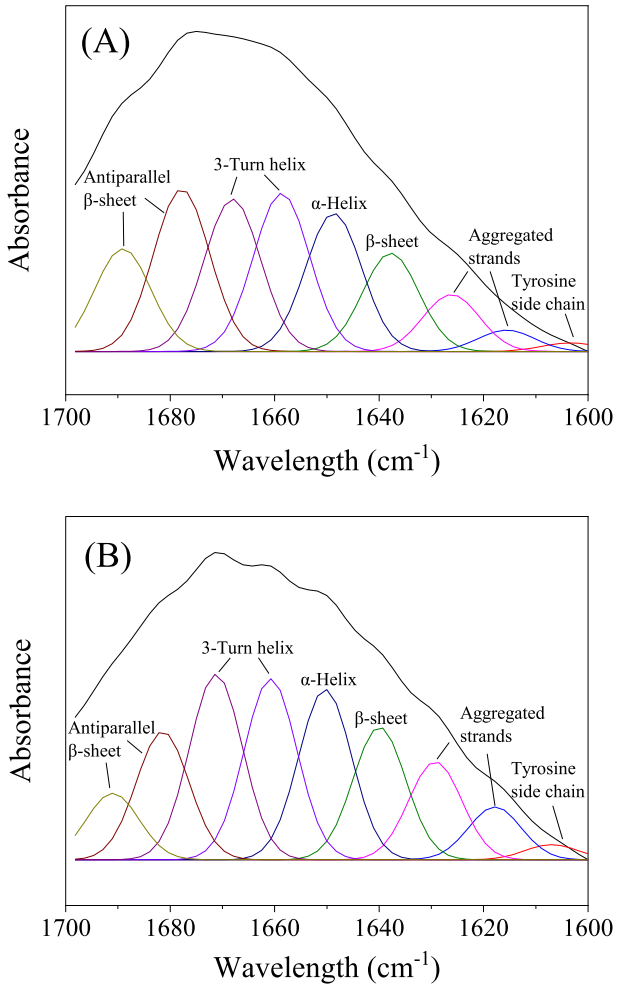

Fig. 4. Second derivative resolution enhanced and curve-fitted amide I region (1700-1600 cm^{-1}) for proteins from (A) the pristine EPS and (B) EPS_20-oCP.

could enhance the aggregation, adsorption and biofilm formation of microbial cells, but antiparallel β-structures and random coils could reduce these factors. In addition, the value of α-helix/(β-sheet + random coils) decreased from 1.405 to 0.739, indicating that the EPS had a loose structure and low flocculating ability after reacting with oCP (You et al., 2017). These results imply that the interaction between EPS and oCP could decrease the hydrophobicity and aggregation of activated sludge.

The elemental compositions and functional groups of the pristine EPS and EPS_20-oCP were further detected by XPS to explore which functional groups in EPS were involved in the formation of the EPS-oCP complex. To quantify the variation in the functional

Table 1
Band assignments for the protein secondary structures of EPS.

Wavelength (cm^{-1})	Secondary structures	% area	
		Pristine EPS	EPS_20-oCP
1607–1603	Tyrosine side chain	0.95	1.46
1626–1616	Aggregated strands	8.72	5.12
1640–1629	β-Sheet	10.94	22.4
1645–1640	Random coil	–	–
1650–1649	α-Helix	15.37	16.55
1671–1659	3-Turn helix	34.55	35.58
1691–1678	Antiparallel β-sheet/aggregated strands	29.47	18.89

groups of the EPS with or without oCP, the C1s and O1s were determined via the high-resolution XPS spectra. The presence of C1s peaks and O1s peaks in the pristine EPS and EPS_20-oCP are illustrated in Fig. 5, and the assignment and quantification of these XPS spectral bands are listed in Table 2.

The C1s peak of the pristine EPS could be resolved into three component peaks (Fig. 5A). The peak at 284.30 eV, which is regarded as aliphatic C–C and C–H bonds (C–C, C–H) from lipids or amino acid side chains, accounted for the largest percentage in the spectral band (55.55%). The peak at 285.11 eV was attributed to C–O or C–N from ether, ethanol or amine groups of proteins (Lin et al., 2016; Yuan et al., 2011). However, the C=O or O–C–O (286.80 eV), attributed to carboxylate, carbonyl, amide, acetal, or hemiacetal groups, presented a lowest percentage in the spectral band (4.46%). The O1s peak of the pristine EPS was resolved in two component peaks and is presented in Fig. 5C. The O1s peak at 530.5 eV (31.39%) was assigned to the O double bonded to C (O=C), as in carboxylate, carbonyl, ester, or amide. The second O1s peak at 531.90 eV (68.61%) was mainly attributed to C–O, as in alcohols, hemiacetal, or acetal groups (Sun et al., 2011).

The C1s and O1s peaks of the EPS_20-oCP are shown in Fig. 5B and D. The C1s peaks at 284.30, 285.11, and 286.80 eV were slightly shifted to 284.40, 285.20 and 287.00 eV, respectively, indicating that the electronic density around C in C–(O,N) and C=O increased and the electronic density around C in C–(C,H) decreased. The O1s peaks at 530.50 and 531.90 eV were shifted to 530.65 and 532.20 eV, respectively, suggesting that the electron cloud around the oxygen atom was transferred to carbon or hydrogen atoms (Song et al., 2014). This observation implies that the carboxyl, carbonyl, amine, and hydroxyl groups of EPS were involved in the formation of the EPS-oCP complex, which was in agreement with the FTIR analytical results.

3.4. NMR results

The ^{1}H NMR spectrum of the pristine EPS is delineated in Fig. 6A. The weak peaks in the region of 8.0–7.5 ppm were attributed to the aromatic ring structure of EPS (De Sousa et al., 2008). The strong signals at 4.0–3.0 ppm represented hydrogen in the –OH group of the polysaccharides and proteins in EPS. The dispersed weak peaks in the ^{1}H chemical shift range of 3.0–0.5 ppm represented the saturated hydrogen of the alkyl group. The peak at 4.66 ppm was attributed to the D_2O.

The ^{1}H NMR spectrum of EPS interacting with 20 mg/L oCP is shown in Fig. 6B. Some changes in the hydrogen signals were observed in comparing the spectrum of EPS_20-oCP with the spectrum of the pristine EPS. The positions of the hydrogen peak were not shifted, but the intensity of peaks at 1.25–1.0 and 3.75–3.25 increased after the dosage of oCP. This result indicated a decrease in electron density around the oxygen atoms and an increase in electron density around the hydrogen atoms in the hydroxyl groups (Song et al., 2014). Therefore, the hydroxyl groups in oCP and EPS were involved mainly in the reaction between oCP and EPS.

Table 2
Binding energies (eV), assignments, and quantization of XPS spectral bands of the pristine EPS and EPS_20-oCP.

Element	EPS		EPS_20-oCP		Assignments
	Peak (eV)	atomic(%)	peak (eV)	atomic (%)	
C1s	284.30	55.55	284.40	53.21	C-(C,H)
C1s	285.11	39.99	285.20	40.21	C-(O,N)
C1s	286.80	4.46	287.00	6.58	C=O,O–C–O
O1s	530.50	31.39	530.65	35.76	C=O
O1s	531.90	68.61	532.20	64.24	C–O–C,C–O–H

3.5. The oCP -EPS interaction mechanisms

EPS are complex matrix materials secreted by microorganisms in the wastewater treatment process and can interact with different organic matters in wastewater. Recently, the interaction mechanisms between EPS and various pollutants, e.g., heavy metal or micro-pollutants, in wastewater have been heavily investigated (Sheng et al., 2013; Xu et al., 2013; Wang et al., 2018a). Two types of mechanisms have been reported for the binding reactions between heavy metals and EPS, including electrostatic interactions and complexing bonds (Sheng et al., 2013). Differently, hydrophobic

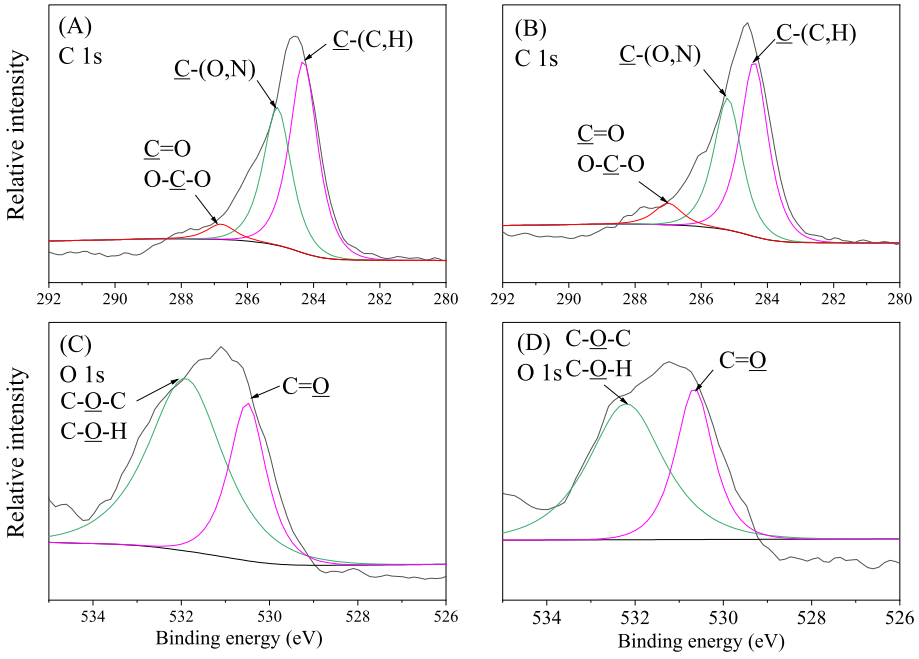

Fig. 5. XPS spectra of (A, C) the pristine EPS, and (B, D) EPS_20-oCP.

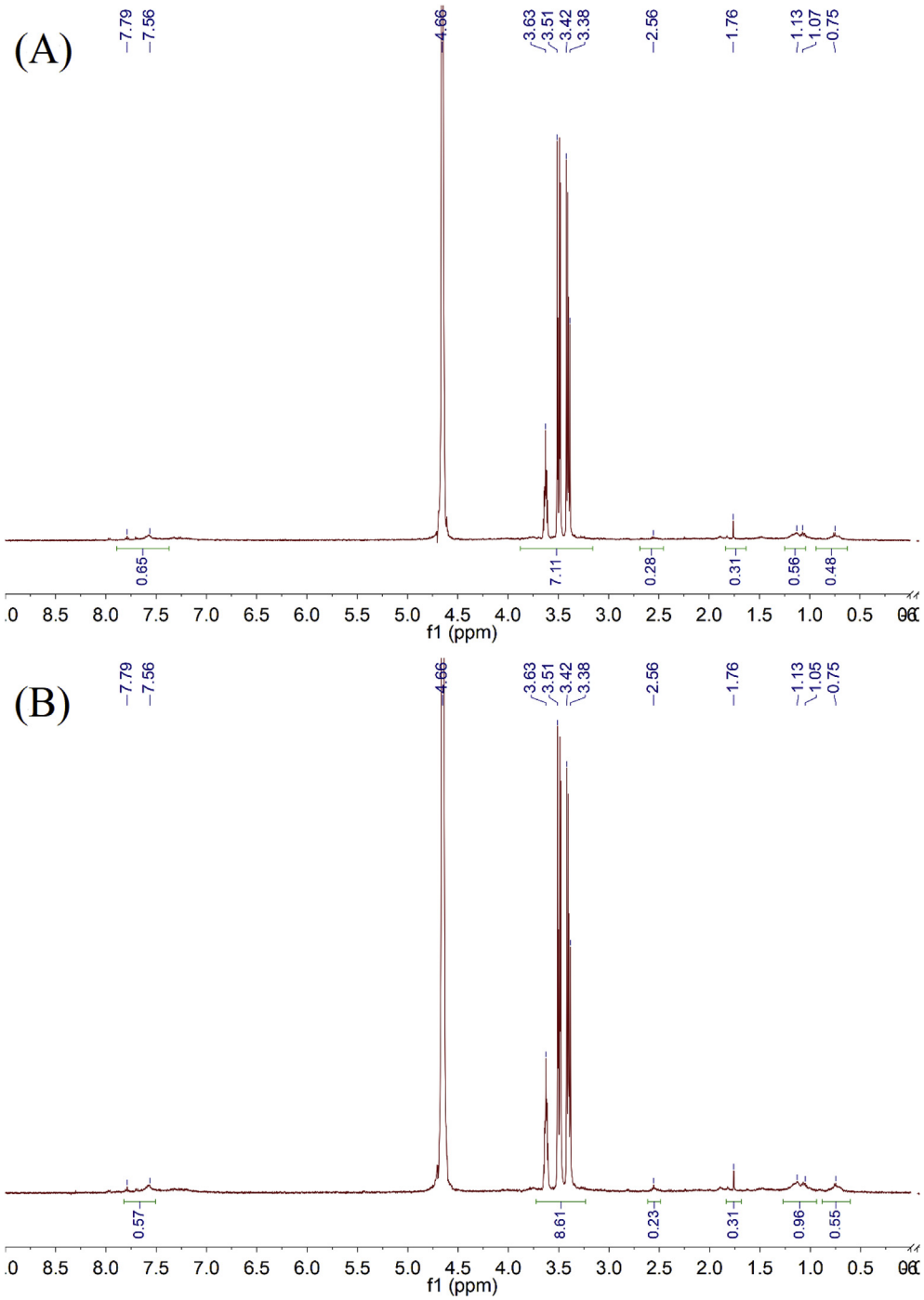

Fig. 6. ^{1}H NMR spectrum of (A) the pristine EPS, and (B) EPS_20-oCP.

interaction was found to play a crucial role in the interaction between EPS and organic pollutants (Xu et al., 2013). In the interaction between sulfamethazine and the proteins in EPS, hydrophobic interaction was the main driving force of the binding process (Xu et al., 2013). Wang et al. (2018a) also observed that the interactions between EPS and sulfamethizole were attributed mainly to the proteins in EPS. In this study, the EEM result shows that the proteins in the sludge EPS provided binding sites and governed the interactions between oCP and EPS, especially the tyrosine protein-like substances (Fig. 2). Furthermore, the FTIR, XPS and NMR results indicate that the main functional groups, such as carboxyl, carbonyl, amine, and hydroxyl groups, dominated the interaction between oCP and EPS (Figs. 3, 5 and 6). These results suggest that the interaction mechanism between metabolic uncouplers such as oCP and EPS were similar to those between EPS and typical antibiotics such as sulfamethizole.

Our results demonstrate the metabolic uncouplers, which are able to disassociate the energy coupling between catabolism and anabolism and result in the dissipation of certain portions of energy through futile cycles, can be trapped by the tyrosine protein-like substances of EPS produced from activated sludge. Thus, the real effect of the metabolic uncouplers would be reduced due to the secretion of EPS in activated sludge. Since the EPS compositions can be affected by many factors (such as hydrodynamics, dissolved

oxygen concentration, etc.), in the future some strategies should be explored to reduce the tyrosine protein-like substances content in EPS. Thus, the effect of excess sludge reduction can be enhanced, which is useful in biological wastewater treatment systems.

4. Conclusions

The interaction mechanisms between oCP and EPS extracted from activated sludge were explored in this study by using different spectral methods. The EEM result showed that the proteins in the sludge EPS provided binding sites and governed the interactions between oCP and EPS. By analyzing with the fluorescence quenching mechanism, the high value of binding constant indicated that the binding of oCP to EPS was mainly governed by the tyrosine protein-like substances. Furthermore, the changes of the carboxyl, carbonyl, amine, and hydroxyl groups of EPS with the analysis of FTIR, XPS, and ^{1}H NMR indicated that these groups were the main functional groups involved in the formation of the oCP-EPS complex. These results provide useful information to understand the interactions between metabolic uncouplers and EPS of activated sludge and track their fates in biological wastewater treatment systems.

Acknowledgements

This work was supported by the National Natural Science Foundation of China (51578210 and 51878244), the Fundamental Research Funds for the Central Universities (2017B13214), the Guangzhou Key Laboratory of Environmental Exposure and Health (GZKLEEH201603) and the Priority Academic Program Development of Jiangsu Higher Education Institutions (PAPD), China.

Appendix A. Supplementary data

Supplementary data to this article can be found online at https://doi.org/10.1016/j.envpol.2019.02.005.

References

Beech, I., Hanjagsit, L., Kalaji, M., Neal, A.L., Zinkevich, V., 1999. Chemical and structural characterization of exopolymers produced by *pseudomonas* sp. NCIMB 2021 in continuous culture. Microbiology 145, 1491–1497.

Chen, W., Westerhoff, P., Leenheer, J.A., Booksh, K., 2003. Fluorescence excitation-emission matrix regional integration to quantify spectra for dissolved organic matter. Environ. Sci. Technol. 37 (24), 5701–5710.

De Sousa, F.B., Oliveira, M.F., Lula, I.S., Sansiviero, M.T.C., Cortés, M.E., Sinisterra, R.D., 2008. Study of inclusion compound in solution involving tetracycline and β-cyclodextrin by FTIR-ATR. Vib. Spectrosc. 46, 57–62.

Fang, F., Hu, H.L., Qin, M.M., Xue, Z.X., Cao, J.S., Hu, R.Z., 2015. Effects of metabolic uncouplers on excess sludge reduction and microbial products of activated sludge. Bioresour. Technol. 185, 1–6.

Ferrer-Polonio, E., Fernandez-Navarro, J., Alonso-Molina, J.L., Amoros-Munoz, I., Bes-Pia, A., Mendoza-Roca, J.A., 2017. Changes in the process performance, sludge production and microbial activity in an activated sludge reactor with addition of a metabolic uncoupler under different operating conditions. J. Environ. Manag. 203, 349–357.

Frølund, B., Palmgren, R., Keiding, K., Nielsen, P.H., 1996. Extraction of extracellular polymers from activated sludge using a cation exchange resin. Water Res. 30, 1749–1758.

Gostomski, P.A., De Vela, R.J.D., 2018. Metabolic uncouplers for controlling biomass accumulation in biological waste treatment systems. Rev. Environ. Sci. Biotechnol. 17, 1–18.

Guo, W.Q., Yang, S.S., Xiang, W.S., Wang, X.J., Ren, N.Q., 2013. Minimization of excess sludge production by in-situ activated sludge treatment processes-A comprehensive review. Biotechnol. Adv. 31, 1386–1396.

Guo, X.S., Yang, J.M., Liang, Y., Liu, J.X., Xiao, B.Y., 2014. Evaluation of sludge reduction by an environmentally friendly chemical uncoupler in a pilot-scale anaerobic/anoxic/oxic process. Bioproc. Biosyst. Eng. 37, 553–560.

Habibul, N., Chen, W., 2018. Structural response of humic acid upon binding with lead: a spectroscopic insight. Sci. Total. Environ. 643, 479–485.

Havel, H.A., 1996. Spectroscopic methods for determining protein structure in solution. Biol. Plant.

Hu, Y.J., Liu, Y., Zhang, L.X., Zhao, R.M., Qu, S.S., 2005. Studies of interaction between colchicine and bovine serum albumin by fluorescence quenching method. J. Mol. Struct. 750, 174–178.

Jia, F.X., Yang, Q., Liu, X.H., Li, X.Y., Li, B.K., Zhang, L., Peng, Y.Z., 2017. Stratification of extracellular polymeric substances (EPS) for aggregated anammox microorganisms. Environ. Sci. Technol. 51 (6), 3260–3268.

Li, K., Wei, D., Yan, T., Du, B., Wei, Q., 2016a. Response of soluble microbial products and extracellular polymeric substances to the presence of toxic 2,6-dichlirophenol in aerobic granular sludge system. J. Environ. Manag. 183, 594–600.

Li, P., Li, H.C., Li, J., Guo, X.S., Liu, J.X., Xiao, B.Y., 2016b. Evaluation of sludge reduction of three metabolic uncouplers in laboratory-scale anaerobic-anoxic-oxic process. Bioresour. Technol. 221, 31–36.

Lin, D., Ma, W., Jin, Z., Wang, Y., Huang, Q., Cai, P., 2016. Interactions of EPS with soil minerals: a combination study by itc and clsm. Colloids Surf., B 138, 10–16.

Liu, Y., 2003. Chemically reduced excess sludge production in the activated sludge process. Chemosphere 50, 1–7.

Mal, J., Nancharaiah, Y.V., Bera, S., Maheshwari, N., Hullebusch, E.D.V., Lens, P.N.L., 2017. Biosynthesis of cdse nanoparticles by anaerobic granular sludge. Environ. Sci.: Nano 4, 824–833.

Mandal, G., Bhattacharya, S., Ganguly, T., 2009. Investigations to reveal the nature of interactions between bovine hemoglobin and semiconductor zinc oxide nanoparticles by using various optical techniques. Chem. Phys. Lett. 478, 271–276.

Raunkjær, K., Hvitved-Jacobsen, T., Nielsen, P.H., 1994. Measurement of pools of protein, carbohydrate and lipid in domestic wastewater. Water Res. 28, 251–262.

Sheng, G.P., Xu, J., Li, W.H., Yu, H.Q., 2013. Quantification of the interactions between Ca^{2+}, Hg^{2+} and extracellular polymeric substances (EPS) of sludge. Chemosphere 93, 1436–1441.

Sheng, G.P., Yu, H.Q., Li, X.Y., 2010. Extracellular polymeric substances (EPS) of microbial aggregates in biological wastewater treatment systems: a review. Biotechnol. Adv. 28, 882–894.

Sheng, G.P., Yu, H.Q., Yue, Z.B., 2005. Production of extracellular polymeric substances from Rhodopseudomonas acidophila, in the presence of toxic substances. Appl. Microbiol. Biotechnol. 69, 216–222.

Shi, L., Wang, X., Li, N., Huai, C., Liu, J., 2012. Chlorine dioxide catalytic oxidation and online FTIR spectroscopic analysis of simulated o-chlorophenol wastewater. Res. Chem. Intermed. 38 (8), 1781–1790.

Song, C., Sun, X.F., Xing, S.F., Xia, P.F., Shi, Y.J., Wang, S.G., 2014. Characterization of the interactions between tetracycline antibiotics and microbial extracellular polymeric substances with spectroscopic approaches. Environ. Sci. Pollut. Res. Int. 21 (3), 1786–1795.

Song, W.J., Mu, G.J., Zhang, D.Y., Pan, X.L., 2010. Interaction of acetamiprid with extracellular polymeric substances (EPS) from activated sludge: a fluorescence study. Afr. J. Biotechnol. 9, 7667–7673.

Sun, X.F., Wang, S.G., Cheng, W., Fan, M.H., Tian, B.H., Gao, B.Y., Li, X.M., 2011. Enhancement of acidic dye biosorption capacity on poly(ethylenimine) grafted anaerobic granular sludge. J. Hazard Mater. 189, 27–33.

Wang, L.F., Li, Y., Wang, L., Zhang, H.J., Zhu, M.J., Zhang, P.S., Zhu, X.X., 2018a. Extracellular polymeric substances affect the responses of multi-species biofilms in the presence of sulfamethizole. Environ. Pollut. 235, 283–292.

Wang, L.L., Wang, L.F., Ren, X.M., Ye, X.D., Li, W.W., Yuan, S.J., Sun, M., Sheng, G.P., Yu, H.Q., Wang, X.K., 2012. pH dependence of structure and surface properties of microbial EPS. Environ. Sci. Technol. 46, 737–744.

Wang, X., Song, W., Qian, H., Zhang, D., Pan, X., Gadd, G.M., 2018b. Stabilizing interaction of exopolymers with nano-Se and impact on mercury immobilization in soil and groundwater. Environ. Sci.: Nano 5, 456–466.

Wei, L.L., Zhao, Q.L., Hu, K., Lee, D.J., Xie, C.M., Jiang, J.Q., 2011. Extracellular biological organic matters in sewage sludge during mesophilic digestion at reduced hydraulic retention time. Water Res. 45, 1472–1480.

Xiao, R., Yang, X., Li, M., Li, X., Wei, Y., Cao, M., Ragauskas, A., Thies, M., Ding, J.H., Zheng, Y., 2018. Investigation of composition, structure and bioactivity of extracellular polymeric substances from original and stress-induced strains of *Thraustochytrium striatum*. Carbohydr. Polym. 195, 515–524.

Xing, X.C., Wang, H.B., Hu, C., Liu, L.Z., 2018. Effects of phosphate-enhanced ozone/biofiltration on formation of disinfection byproducts and occurrence of opportunistic pathogens in drinking water distribution systems. Water Res. 139, 168–176.

Xu, J., Sheng, G.P., Ma, Y., Wang, L.F., Yu, H.Q., 2013. Roles of extracellular polymeric substances (EPS) in the migration and removal of sulfamethazine in activated sludge system. Water Res. 47, 5298–5306.

Yin, C.Q., Meng, F.G., Chen, G.H., 2015. Spectroscopic characterization of extracellular polymeric substances from a mixed culture dominated by ammonia-oxidizing bacteria. Water Res. 68, 740–749.

You, G.X., Wang, P.F., Hou, J., Wang, C., Xu, Y., Miao, L.Z., Lv, B., Yang, Y.Y., Liu, Z.L., Zhang, F., 2017. Insights into the short-term effects of CeO_2, nanoparticles on sludge dewatering and related mechanism. Water Res. 118, 93–103.

Yuan, S.J., Sun, M., Sheng, G.P., Li, Y., Li, W.W., Yao, R.S., Yu, H.Q., 2011. Identification of key constituents and structure of the extracellular polymeric substances excreted by *Bacillus megaterium* TF10 for their flocculation capacity. Environ. Sci. Technol. 45, 1152–1157.

Zhang, H.Q., Jia, Y.Y., Khanal, S.K., Lu, H., Fang, H.T., Zhao, Q., 2018. Understanding the role of extracellular polymeric substances on ciprofloxacin adsorption in aerobic sludge, anaerobic sludge, and sulfate-reducing bacteria sludge systems. Environ. Sci. Technol. 52, 6476–6486.